Original Article | Cardiovascular Imaging

eISSN 2005-8330
https://doi.org/10.3348/kjr.2020.1218
Korean J Radiol 2021;22(8):1266-1278

Korean Journal of Radiology
KJR

A New Method for Aortic Valve Planimetry with High-Resolution 3-Dimensional MRI and Its Comparison with Conventional Cine MRI and Echocardiography for Assessing the Severity of Aortic Valvular Stenosis

Hae Jin Kim[1, 2], Yeon Hyeon Choe[1, 3], Sung Mok Kim[1, 3], Eun Kyung Kim[3, 4], Mirae Lee[5], Sung-Ji Park[3, 4], Joonghyun Ahn[6], Keumhee C. Carriere[7]

[1]Department of Radiology, Samsung Medical Center, Sungkyunkwan University School of Medicine, Seoul, Korea; [2]Department of Radiology, Daejeon Eulji Medical Center, Eulji University School of Medicine, Daejeon, Korea; [3]HVSI Imaging Center, Heart Vascular Stroke Institute, Samsung Medical Center, Sungkyunkwan University School of Medicine, Seoul, Korea; [4]Division of Cardiology, Department of Medicine, Samsung Medical Center, Sungkyunkwan University School of Medicine, Seoul, Korea; [5]Division of Cardiology, Department of Medicine, Samsung Changwon Hospital, Sungkyunkwan University School of Medicine, Changwon, Korea; [6]Statistics and Data Center, Samsung Medical Center, Seoul, Korea; [7]Department of Mathematical and Statistical Sciences, University of Alberta, Edmonton, AB, Canada

Objective: We aimed to compare the aortic valve area (AVA) calculated using fast high-resolution three-dimensional (3D) magnetic resonance (MR) image acquisition with that of the conventional two-dimensional (2D) cine MR technique.

Materials and Methods: We included 139 consecutive patients (mean age ± standard deviation [SD], 68.5 ± 9.4 years) with aortic valvular stenosis (AS) and 21 asymptomatic controls (52.3 ± 14.2 years). High-resolution T2-prepared 3D steady-state free precession (SSFP) images (2.0 mm slice thickness, 10 contiguous slices) for 3D planimetry (3DP) were acquired with a single breath hold during mid-systole. 2D SSFP cine MR images (6.0 mm slice thickness) for 2D planimetry (2DP) were also obtained at three aortic valve levels. The calculations for the effective AVA based on the MR images were compared with the transthoracic echocardiographic (TTE) measurements using the continuity equation.

Results: The mean AVA ± SD derived by 3DP, 2DP, and TTE in the AS group were 0.81 ± 0.26 cm^2, 0.82 ± 0.34 cm^2, and 0.80 ± 0.26 cm^2, respectively (p = 0.366). The intra-observer agreement was higher for 3DP than 2DP in one observer: intraclass correlation coefficient (ICC) of 0.95 (95% confidence interval [CI], 0.94–0.97) and 0.87 (95% CI, 0.82–0.91), respectively, for observer 1 and 0.97 (95% CI, 0.96–0.98) and 0.98 (95% CI, 0.97–0.99), respectively, for observer 2. Inter-observer agreement was similar between 3DP and 2DP, with the ICC of 0.92 (95% CI, 0.89–0.94) and 0.91 (95% CI, 0.88–0.93), respectively. 3DP-derived AVA showed a slightly higher agreement with AVA measured by TTE than the 2DP-derived AVA, with the ICC of 0.87 (95% CI, 0.82–0.91) vs. 0.85 (95% CI, 0.79–0.89).

Conclusion: High-resolution 3D MR image acquisition, with single-breath-hold SSFP sequences, gave AVA measurement with low observer variability that correlated highly with those obtained by TTE.

Keywords: *Aortic valve; Aortic stenosis; Planimetry; Cardiac magnetic resonance imaging, Echocardiography*

INTRODUCTION

The severity of aortic valvular stenosis (AS) can be assessed with Doppler echocardiography by measuring the AS jet velocity, and the aortic valve area (AVA) can be assessed by either the continuity equation or direct

Received: October 07, 2020 **Revised:** December 1, 2020 **Accepted:** December 31, 2020
Corresponding author: Yeon Hyeon Choe, MD, PhD, Department of Radiology and HVSI Imaging Center, Heart Vascular Stroke Institute, Samsung Medical Center, Sungkyunkwan University School of Medicine, 81 Irwon-ro, Gangnam-gu, Seoul 06351, Korea.
• E-mail: yhchoe@skku.edu

Korean Journal of Radiology
KJR

planimetry [1-5]. Doppler echocardiography does not provide direct information on pressure; instead, it relies on the measurement of the left ventricular outflow tract (LVOT). It also requires good imaging windows for accurate diagnosis [5,6].

More recently, cardiovascular magnetic resonance (CMR) has emerged as a complementary tool for noninvasively evaluating AS [2,7-13]. Studies have shown its usefulness for the assessment of AVA and aortic hemodynamic parameters, either by planimetry of cine anatomical images or by analyzing velocity-encoded images using the continuity equation [14,15]. Given that the aortic valve is continuously moving, it is difficult to depict the exact phase and location of the maximal systolic opening on two-dimensional (2D) cine images placed perpendicular to the valve flow. Previous studies have indicated that planimetry-based AVA measurement may be effective when using variable sequences such as balanced steady-state free precession (SSFP) gradient-echo or phase-contrast imaging [16,17]. However, most cardiovascular MR studies of direct planimetry of stenotic aortic valves have shown that measurement errors occur, especially in heavily calcified aortic valves. This is because of problems related to the voxel size relative to the AVA, low signals in calcifications and turbulences close to the borders of the aortic leaflets, and irregularities in the shape of the stenotic orifice [18].

We hypothesized that the novel application of aortic planimetry with high-spatial-resolution three-dimensional (3D) MR images would provide faster and more reliable information on aortic valve planimetry than 2D cine MR images. The aim of this study was, therefore, to test whether high-resolution 3D MR image acquisition with single-breath-hold SSFP sequences could facilitate a reproducible and accurate evaluation of AVA.

MATERIALS AND METHODS

Study Population

We performed a prospective study of 142 consecutive patients who underwent CMR and echocardiography, with varying degrees of AS at our institution between January 2012 and May 2015. CMR was indicated in those patients for accurately assessing LV and aortic valvular function, the degree of myocardial fibrosis, and stress myocardial perfusion [19]. Three patients were excluded because of poor image quality, leaving 139 patients (age, 68.5 ± 9.4 years; 72 male and 67 female) for the analysis. For comparison, we included 21 asymptomatic controls (age, 52.3 ± 14.2 years; 19 male and 2 female) (Fig. 1, Table 1). The study was approved by our Institutional Review Board, and written informed consent was obtained from each patient (IRB No. 2012-01-014).

Acquisition of MRI Data

All patients underwent cardiac MRI during repeated breath holding using a 1.5T scanner (Magnetom Avanto, Syngo MR B17 version; Siemens Healthineers) with a 32-channel phased-array receiver coil. High-resolution 3D SSFP images (3D planimetry [3DP]; 2.0 mm slice thickness, 10 contiguous slices; image matrix, 256 x 209) were acquired within a single breath hold during mid-systole. The imaging parameters were as follows: repetition time

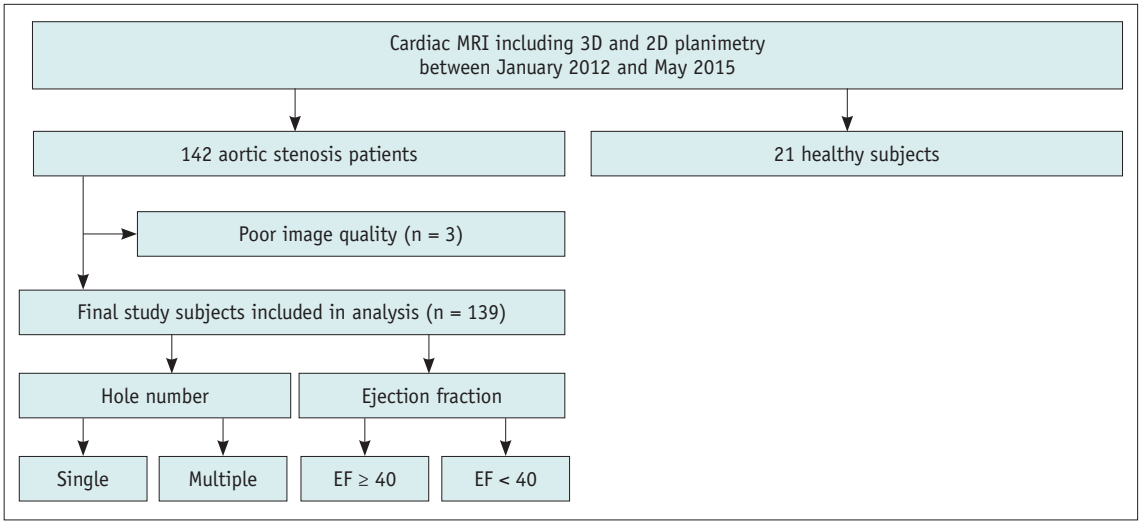

Fig. 1. Participant flow diagram. EF = ejection fraction, 2D = two-dimensional, 3D = three-dimensional

https://doi.org/10.3348/kjr.2020.1218

Table 1. Participant Characteristics

Variable	Patients (n = 139)	Control (n = 21)	*P*
Age, years	68.5 ± 9.4	52.3 ± 14.2	0.026
Male, %	72 (51.8)	19 (90.4)	0.011
Body mass index, kg/m^2	24.2 ± 3.4	24.3 ± 3.4	0.126
Body surface area, m^2	1.6 ± 0.2	1.8 ± 0.2	0.417
AS grade, %			
Mild	2 (1.4)	0 (0)	< 0.001
Moderate	22 (15.8)	0 (0)	0.084
Severe	115 (82.7)	0 (0)	< 0.001
AR grade, %			
Mild	17 (12.2)	8 (38.1)	0.063
Moderate	8 (5.8)	0 (0)	0.307
Severe	2 (1.4)	0 (0)	0.348
Associated findings			
Bicuspid aortic valve, %	47 (33.8)	2 (9.52)	0.173
Ejection fraction, %	61.0 ± 14.2	64.4 ± 17.2	0.994
End-diastolic volume, mL	154.2 ± 61.2	183.0 ± 98.9	0.832
End-systolic volume, mL	65.2 ± 48.1	87.9 ± 90.7	0.752
Stroke volume, mL	89.1 ± 29.8	95.3 ± 28.5	0.894
Cardiac output, L/min	6.4 ± 5.4	6.8 ± 3.1	0.331
End-diastolic wall mass, g	161.8 ± 64.2	133.9 ± 42.0	0.927

Data are mean ± standard deviation or number of patients with the percentage in parentheses. AR = aortic regurgitation, AS = aortic stenosis

(TR), 3.8 ms; echo time (TE), 1.6 ms; flip angle, 90°; T2 preparation time, 40 ms; slab thickness, 20 mm; field-of-view, 320 x 289 mm; imaging time, 14 seconds; generalized autocalibrating partially parallel acquisitions (GRAPPA) factor, 3; slice resolution, 50%; slice thickness, 2 mm; pixel spacing, 1.39 x 1.25 mm. The mean RR interval was 896 ms and the image acquisition duration was 190 ms. The data were acquired at 107–297 ms from the R peaks during the systolic phase (Fig. 2). For 3DP, ten contiguous slices were taken perpendicular to the longitudinal direction of the ascending aorta at the level of the aortic valve using a mid-systolic longitudinal aortic valve cine MR image as a scout view (Fig. 3). The imaging slab was positioned to capture the mid-systolic aortic valve images in the middle. Finally, 3D multiplanar reconstruction was performed using commercial software (Aquaris iNtuition version 4.4.11, TeraRecon). From the 3D volume data, the optimal plane for measuring AVA was determined. Representative examples of 3DP are shown in Figure 4 and Supplementary Movie.

We also performed SSFP cine MRI (2D planimetry [2DP]) and velocity-encoded cine (VENC) MRI at three levels of the aortic valve. SSFP was used to obtain 2D images in the prescribed planes during multiple phases throughout the cardiac cycle. Cine images were acquired in three

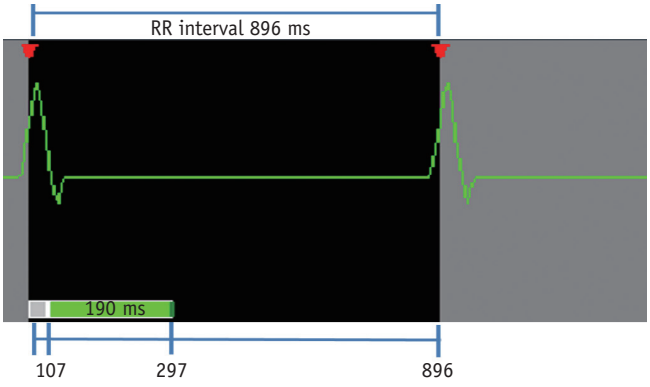

Fig. 2. Cardiovascular magnetic resonance image acquisition scheme for three-dimensional planimetry. Image acquisition duration was 190 ms. Data were acquired at 107–297 ms after the R peak during the systolic phase.

short-axis views covering the AVA, from the LVOT to the ascending aorta at 6-mm intervals, using a segmented SSFP sequence. To produce an SSFP cine image throughout systole and diastole, the images were obtained over several cardiac cycles in multiple breath holds (Fig. 5). Acquisition parameters for the cine images and VENC imaging are described in Supplementary.

Transthoracic echocardiography (TTE) (M-mode, 2D, and Doppler) was performed using commercially available

https://doi.org/10.3348/kjr.2020.1218

Korean Journal of Radiology
KJR

equipment (Vivid 7, GE Medical System; Acuson 512, Siemens Healthineers; or Sonos 5500, Philips Healthcare). The continuity equation was used to calculate AVA, using the LVOT diameter, LVOT peak velocity measured by pulsed-wave Doppler, and the highest aortic valve continuous-wave Doppler peak velocity obtained from the apical or right

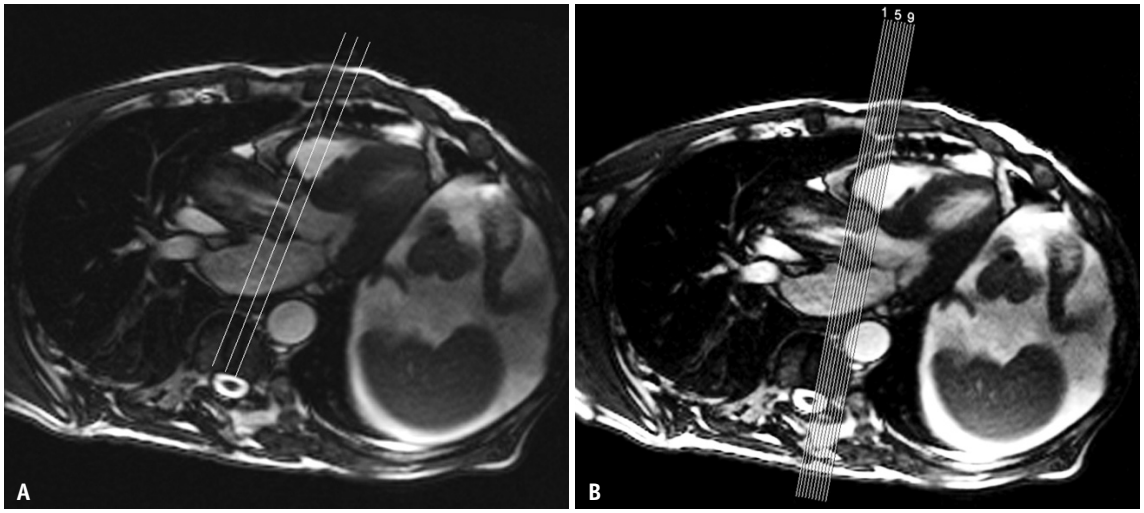

Fig. 3. Image prescription of 2D and 3D planimetry sequence.
A. Cine images were acquired in three short-axis views covering the aortic valve area, from the left ventricular outflow tract to the ascending aorta at 6-mm intervals, using a segmented steady-state free precession sequence. **B.** In 3D planimetry, ten contiguous slices were obtained in a single breath hold perpendicular to the long axis of the ascending aorta in the aortic valve plane. The scout view for this acquisition was the mid-systolic phase image of the 3-chamber view cine MRI. The most stenotic portion of the aortic valve was targeted for images in the middle of the slab, corresponding to the mid-systolic phase. 2D = two-dimensional, 3D = three-dimensional

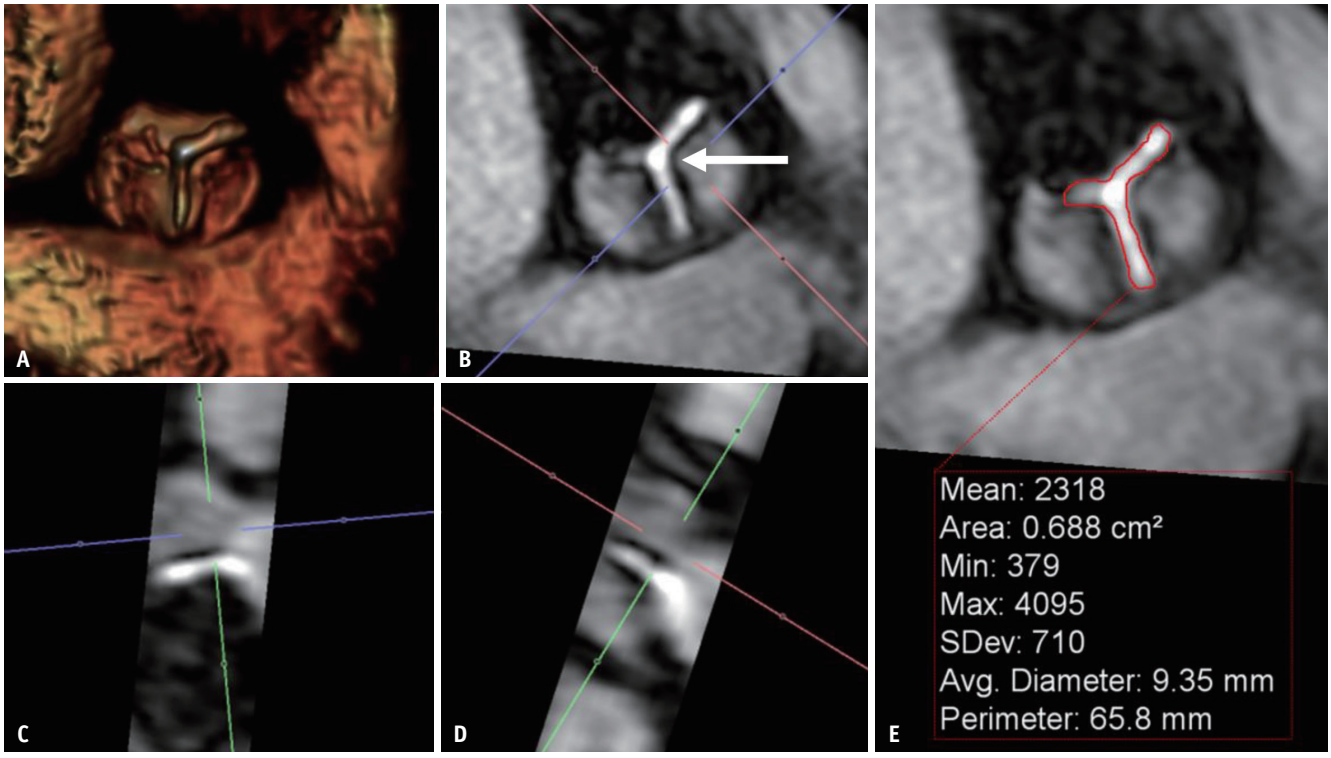

Fig. 4. Representative examples of 3D planimetry reconstructed using commercial software (iNtuition, TeraRecon).
A. The volume-rendering image shows the 3D structure of the aortic valve. **B-D.** Two directional cross-sectional images, taken perpendicular to the aortic valve, were used for reconstruction. Note that there is a high-velocity jet (arrow) with high contrast. **E.** We measured the maximum area of the aortic valve at mid-systole. Avg = average, SDev = standard deviation, 3D = three-dimensional

https://doi.org/10.3348/kjr.2020.1218

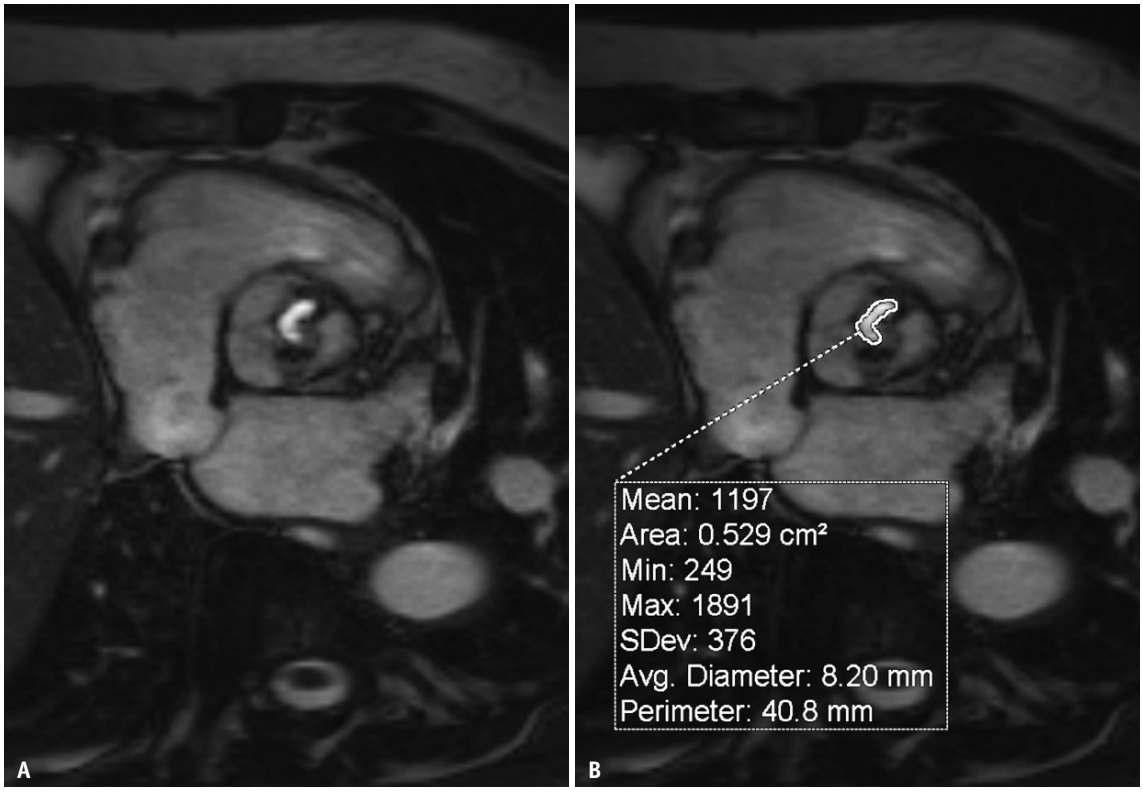

Fig. 5. A representative example of 2D planimetry for cine MRI.
A. The steady-state free precession sequence produced a 2D image during multiple phases throughout the cardiac cycle. **B.** We drew a line along the edge of the maximally open aortic valve on the cine image. 2D = two-dimensional

parasternal window (averaged over three beats).

Analysis of MRI Data

All scans were analyzed by two experienced observers (OB1 and OB2, 6 and 26 years' experience in cardiovascular MRI, respectively) who were blinded to all clinical information, using the iNtuition commercial software (TeraRecon) and a Syngo MR B13 workstation (Siemens Healthineers).

Image Quality of the Aortic Valve

Image quality was assessed using a four-point scale, as follows: 1 = severe blurring of images; 2 = moderate blurring of valve contours; 3 = mild blurring of valve contours; 4 = excellent, with no artifact. Grades 3 and 4 indicated diagnostic quality (Fig. 6). Image quality was expected to be affected by the amount of aortic valve calcification.

Evaluation of AVA

Both observers measured AVA using both 2DP and 3DP in the AS and control groups. To measure AVA using 3DP, we sent the MR images to a TeraRecon workstation, performed 3D image reconstruction of the valve, and calculated the area (cm^2) by positioning a crosshair along the edges of the open aortic valves at mid-systole (Fig. 4). To measure the AVA using 2DP, we drew lines along the edges of the open aortic valves at mid-systole (Fig. 5). To assess intra-observer variability for the interpretation of the aortic valve, each observer performed AVA measurements twice at a one-month interval.

We compared the AVA measurements by 3DP and 2DP and TTE. For TTE, the AVA was calculated using the continuity equation [20]. We found 31 cases with multiple orifices in the AS group (31 multiple-orifice patients; 108 single-orifice patients). We measured and added stenotic orifice areas for the calculation of AVA. We compared the measurement accuracies of the 3DP and 2DP techniques for both the multiple-orifice and single-orifice groups. In addition, we divided the whole study population into two groups based on LV function. Based on an ejection fraction (EF) of 40%, we found that 123 patients had an EF of ≥ 40% and 17 patients had an EF of < 40%. We compared the measurement accuracies for the 3DP and 2DP techniques in both groups.

Finally, we calculated the maximum transvalvular peak

https://doi.org/10.3348/kjr.2020.1218

Korean Journal of Radiology
KJR

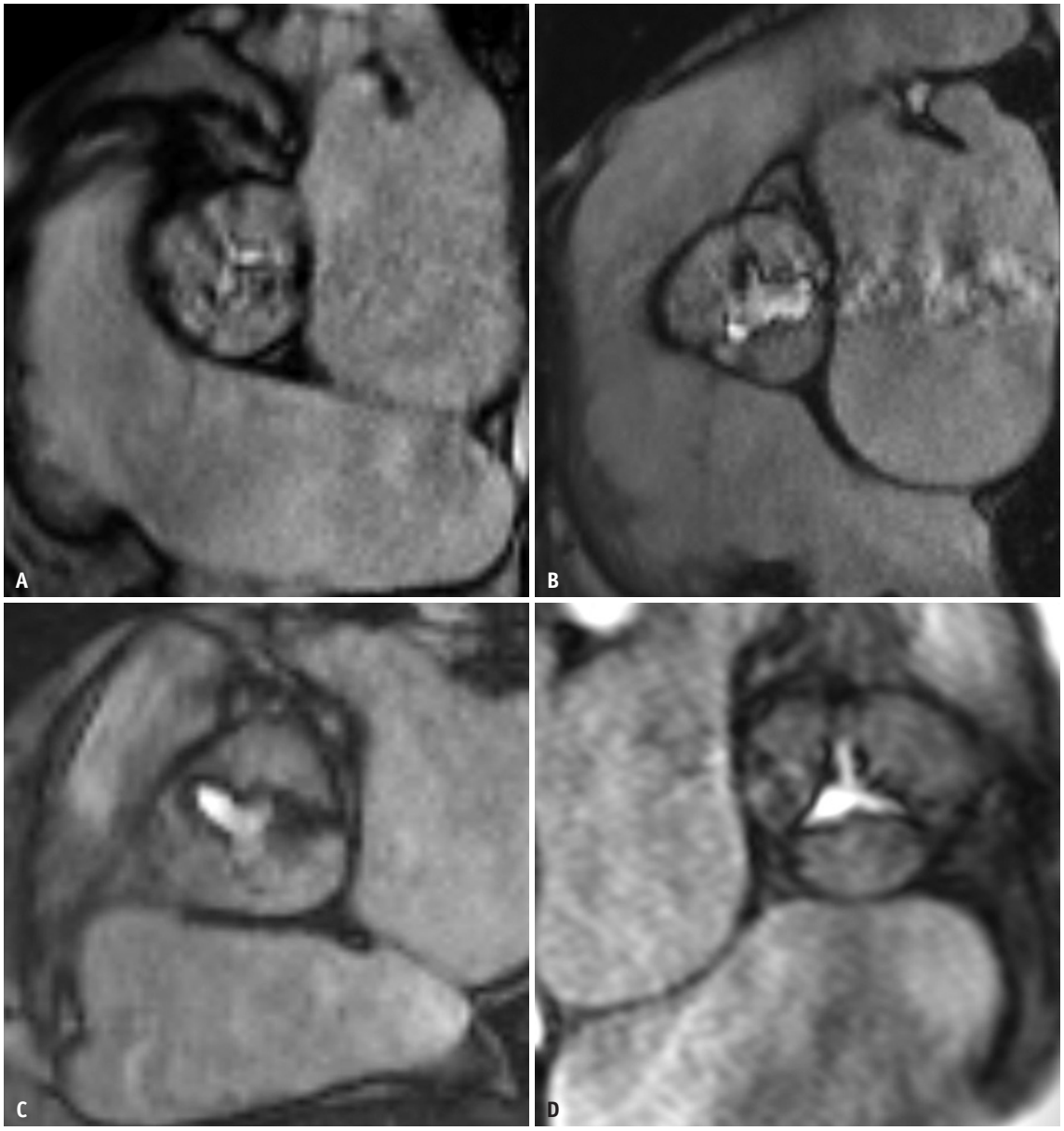

Fig. 6. Assessment of image quality for 2D and 3D planimetry.
A-D. Image quality was assessed using a four-point scale as follows. **A.** 1 = severe blurring of images. **B.** 2 = moderate blurring of valve contours. **C.** 3 = mild blurring of valve contours. **D.** 4 = excellent, with no artifact. Grades 3 and 4 indicated diagnostic quality. 2D = two-dimensional, 3D = three-dimensional

systolic velocity at the aortic valve using VENC imaging. We, subsequently, assessed the correlation between the AVAs obtained using the two techniques and the peak systolic velocity for the valve-obtained VENC imaging (i.e., 3D AVA or 2D AVA vs. peak systolic velocity) based on the hypothesis that the AVA is narrower if the transvalvular flow jet pressure is higher.

Statistical Analysis

To compare the AVAs obtained by the 3DP and 2DP techniques with that obtained by TTE, we measured the intraclass correlation coefficients (ICCs) for the intra- and inter-observer agreements. Bland-Altman plots were constructed to facilitate the assessment of the sources of disagreements. The qualities of the 2DP and 3DP images were compared using weighted-kappa statistics, which adjusted the unweighted kappa for asymmetry of the two-way table for image quality rating data. The various ICCs and image qualities were compared using two-sample *t* tests, applying the central limit theorem for large samples.

https://doi.org/10.3348/kjr.2020.1218

In addition, we considered adjusting for confounding factors in the measurements using the generalized estimating equation approach to analyze the repeated-measures data between the two observers. All statistical analyses were conducted using R software version 3.2.2. All *p* values of < 0.05 were considered statistically significant.

RESULTS

Demographics and Basic Patient Characteristics

The clinical characteristics of the study population are summarized in Table 1. No differences were evident between the AS and control groups. Aortic valve replacement was performed in 105 of the 139 patients in the AS group. Two, 22, and 115 patients had mild, moderate, and severe AS, respectively. The typical surgical findings were leaflet thickening, leaflet calcification, degenerative changes, and annular calcification. Of the 22 patients who did not undergo surgery, 21 had moderate AS, and one refused surgery.

Image Quality

Table 2 lists the mean image quality scores ± standard deviation (SD) for 2DP and 3DP. The mean image quality for 3DP was higher than that for 2DP without statistical significance (3.6 ± 0.6 vs. 3.3 ± 0.7 [p = 0.53] in the AS group; 3.0 ± 0.4 vs. 2.8 ± 0.4 [p = 0.61] in the control group).

Analysis of AVA

The Bland-Altman plot (Fig. 7) indicated that no obvious trend in the two methods and TTE or the repeated measures observed by the same observer. The mean 3D AVA results for each observer (OB1 and OB2) during the first (OB1–1 and OB2–1) and second (OB1–2 and OB2–2) assessments are shown in Table 2. The mean ± SD of AVAs according to the average of OB1 and OB2 in the AS group measured by 3DP, 2DP, and TTE were 0.81 ± 0.26 cm^2, 0.82 ± 0.34 cm^2, and 0.80 ± 0.26 cm^2, respectively (p = 0.366). In the control group, the AVAs by 3DP and 2DP were 3.7 ± 0.7 cm^2 and 4.0 ± 0.8 cm^2, respectively (p = 0.046).

In total, four measurements were obtained for each method, and 3DP showed a higher degree of agreement with echocardiographic AVA than 2DP. The ICCs for 3DP were as follows: OB1–1 = 0.9 (95% CI, 0.85–0.93); OB1–2 = 0.93 (95% CI, 0.90–0.95); OB2–1 = 0.73 (95% CI, 0.63–0.81); OB2–2 = 0.71 (95% CI, 0.60–0.79) (p < 0.001). The ICCs for 2DP were as follows: OB1–1 = 0.83 (95% CI, 0.76–0.88); OB1–2 = 0.85 (95% CI, 0.79–0.89); OB2–1 = 0.72 (95% CI, 0.61–0.80); OB2–2 = 0.72 (95% CI, 0.61–0.80) (p < 0.001). In particular, there was a high concordance among patients with an EF of ≥ 40% and all patients. The agreement between 3DP AVA and echocardiography was lower for patients with EFs of < 40% than for those with higher EFs, but there was no significant difference in measurements between the 3DP and 2DP techniques (Table 3). The inter- and intra-observer agreements were excellent for all the groups (ICC, 0.87–0.98) (p < 0.001) (Table 2).

Table 2. Comparison of AVA by Two Methods (3D Planimetry vs. 2D Planimetry)

Planimetry	3D AVA			2D AVA		
	All Patients (n = 139)	EF ≥ 40 (n = 122)	EF < 40 (n = 17)	All Patients (n = 139)	EF ≥ 40 (n = 122)	EF < 40 (n = 17)
Image quality*	3.6 ± 0.6			3.3 ± 0.7		
AVA (cm^2) according to average of OB1 and OB2*	0.81 ± 0.26			0.82 ± 0.34		
AVA (cm^2) by single OB*						
OB1–1	0.79 ± 0.24	0.80 ± 0.25	0.71 ± 0.18	0.85 ± 0.34	0.86 ± 0.35	0.79 ± 0.33
OB1–2	0.77 ± 0.23	0.78 ± 0.24	0.74 ± 0.22	0.76 ± 0.29	0.76 ± 0.28	0.82 ± 0.33
OB2–1	0.84 ± 0.28	0.84 ± 0.29	0.84 ± 0.22	0.83 ± 0.36	0.82 ± 0.37	0.85 ± 0.31
OB2–2	0.84 ± 0.27	0.84 ± 0.27	0.84 ± 0.23	0.84 ± 0.35	0.83 ± 0.35	0.89 ± 0.32
Intra-OB agreement (ICC)						
OB1	0.95 (95% CI, 0.94–0.97)			0.87 (95% CI, 0.82–0.91)		
OB2	0.97 (95% CI, 0.96–0.98)			0.98 (95% CI, 0.97–0.99)		
Inter-OB agreement (ICC)	0.92 (95% CI, 0.89–0.94)			0.91 (95% CI, 0.88–0.93)		

OBa-b indicates OB a's bth measurement. *Data are mean ± standard deviation. AVA = aortic valve area, CI = confidence interval, EF = ejection fraction, ICC = intraclass correlation coefficient, OB = observer, 2D = two-dimensional, 3D = three-dimensional

https://doi.org/10.3348/kjr.2020.1218

Korean Journal of Radiology
KJR

The peak systolic velocity on VENC MRI and 3DP or 2DP were significantly and negatively correlated. For each measurement set by the observers, the correlation ranged from -0.46 to -0.50 ($p < 0.001$) and -0.48 to -0.56 ($p < 0.001$) for 3DP and 2DP, respectively, in the AS group.

We identified 31 patients in the AS group who had two or more separate AS orifices (Table 4). In those patients, the TTE AVA values (0.69 ± 0.21 cm^2) tended to be lower than those by 3DP (0.71 ± 0.15 cm^2) or 2DP (0.70 ± 0.17 cm^2). Statistical significance in difference in observer agreement between single-orifice AVA and multiple-orifice AVA was not achieved, because the sample size was small. Although multiple openings were observed with 3DP in 31 cases, no cases exhibited multiple openings on surgery or echocardiography (Fig. 8). The 3D images enabled us to find the most stenotic point of the valve, which can be difficult with 2D images. The ratio of bicuspid valves in the multiple-orifice group was 71% (22 patients).

The observer discrepancies of the ICC and image quality were caused by differences in EF, body mass index, end-

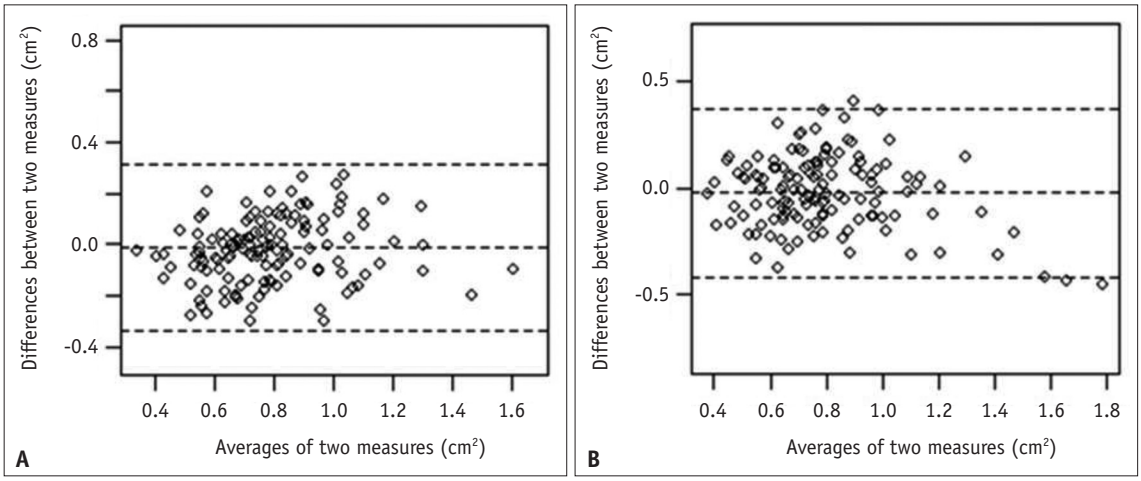

Fig. 7. Bland-Altman plot for interobserver agreement for 3D AVA or 2D AVA and TTE.
The Bland-Altman plot of the averages of the two measures vs. the differences between the two measures indicated that there was no obvious trend in the 3D planimetry and TTE findings **(A)**, as well as those of 2D planimetry and TTE **(B)**. AVA = aortic valve area, TTE = transthoracic echocardiographic, 2D = two-dimensional, 3D = three-dimensional

Table 3. Agreement of Aortic Valve Areas by 3D and 2D Planimetry with that by Echocardiography

	All Patients (n = 139)	EF ≥ 40 (n = 122)	EF < 40 (n = 17)
3D			
OB1	0.92 (95% CI, 0.89–0.95)	0.94 (95% CI, 0.91–0.95)	0.81 (95% CI, 0.48–0.93)
OB2	0.73 (95% CI, 0.62–0.81)	0.74 (95% CI, 0.63–0.82)	0.64 (95% CI, 0.73–0.87)
Average	0.87 (95% CI, 0.82–0.91)	0.88 (95% CI, 0.83–0.92)	0.75 (95% CI, 0.32–0.91)
2D			
OB1	0.87 (95% CI, 0.82–0.91)	0.86 (95% CI, 0.81–0.91)	0.92 (95% CI, 0.79–0.97)
OB2	0.73 (95% CI, 0.62–0.80)	0.7 (95% CI, 0.58–0.79)	0.92 (95% CI, 0.77–0.97)
Average	0.85 (95% CI, 0.79–0.89)	0.84 (95% CI, 0.76–0.88)	0.93 (95% CI, 0.82–0.98)

The results show the intraclass correlation coefficient calculated based on the averages of the repeated measurements of the observers.
CI = confidence interval, EF = ejection fraction, OB = observer, 2D = two-dimensional, 3D = three-dimensional

Table 4. Comparison of Agreement in Single-Orifice AVA and Multi-Orifice AVA by 3D and 2D Planimetry with that by Echocardiography

	Single-Orifice (n = 108)		Multiple-Orifices (n = 31)	
	3D	2D	3D	2D
OB1	0.93 (95% CI, 0.90–0.95)	0.87 (95% CI, 0.81–0.91)	0.83 (95% CI, 0.64–0.92)	0.81 (95% CI, 0.60–0.91)
OB2	0.72 (95% CI, 0.60–0.81)	0.73 (95% CI, 0.60–0.81)	0.66 (95% CI, 0.29–0.84)	0.52 (95% CI, 0.01–0.77)
Average	0.88 (95% CI, 0.82–0.91)	0.85 (95% CI, 0.78–0.90)	0.78 (95% CI, 0.55–0.89)	0.73 (95% CI, 0.44–0.87)

AVA = aortic valve area, CI = confidence interval, OB = observer, 2D = two-dimensional, 3D = three-dimensional

https://doi.org/10.3348/kjr.2020.1218

diastolic volume, cardiac output, and peak flow velocity (Vmax) by TTE for each patient. Specifically, 2DP or 3DP values were higher by 0.0087 ($p < 0.001$) for those with EFs of > 40% than for those with EFs of < 40%. The values were also 0.068 higher ($p = 0.007$) for those with high body mass indexes than for those with low body mass indexes and 0.0023 higher ($p < 0.001$) for a high end-diastolic volume than for a low end-diastolic volume; however, the values were 0.171 lower ($p < 0.001$) for a high Vmax than for a low Vmax.

Among the 139 patients, 99 had severe calcification in the aortic valves (Fig. 9). In these patients, the mean image quality for 3DP was slightly higher than that for 2DP without statistical significance (3.5 ± 0.8 vs. 3.2 ± 0.7 [$p = 0.58$]). The 3DP-derived AVA showed a higher degree of agreement with echocardiographic AVA than the 2DP-derived AVA, with the ICC of 0.87 (95% CI, 0.81–0.88) for 3DP vs. 0.84 (95% CI, 0.75–0.85) for 2DP.

In 47 patients (33.8%), the aortic valves were bicuspid. In these patients, the values of the mean AVA, image quality, and agreement with echocardiography were slightly lower than those of the tricuspid aortic valve (TAV), but three values were not significantly different (ICC for 3DP: bicuspid aortic valve [BAV]) 0.92 [95% CI, 0.86–0.96]; TAV 0.84 [95% CI, 0.75–0.89] [$p = 0.03$], ICC for 2DP: BAV 0.85 [95% CI, 0.74–0.92]; TAV 0.85 [95% 0.77–0.90] [$p = 0.90$]) (Table 5).

DISCUSSION

Our study showed that high-resolution 3D MR image acquisition, with single-breath-hold SSFP sequences, enabled planimetry of AVA in patients with valvular AS. Moreover, this method was more reliable than 2DP by conventional cine MRI. In clinical practice, the evaluation of AS is mainly based on echocardiographic measurements of the effective orifice area (EOA) of the valve, which corresponds to the minimal cross-sectional area of the transvalvular flow jet downstream of the aortic valve. However, echocardiographic measurements are not always feasible, or they may lead to discordant EOA and pressure gradient results (e.g., when measured by TTE) [7].

In the present study, we proposed a new method based on determining AVA directly based on a high-resolution T2-prepared 3D SSFP MR image during breath holding. This method is theoretically more reliable and accurate than the 2D method. The results indicated that there was excellent agreement between AVA estimated by this new method and EOA predicted by echocardiography using the continuity equation. Overall, we found no differences between the means determined by the gold standard (i.e., TTE) and the two observers or between the repeated measures. We concluded that there was excellent consistency and agreement of all the measurements. Compared with 2DP by cine MRI, 3DP produced a better image quality, shorter scan times, and more reliable AVA measurements.

The main advantage of the 3DP method used in this study was that it allowed for comprehensive analysis of the aortic valve structure by providing 3D volume data for AVA. The crosshair could also be aligned along the plane of the most stenotic aortic valve orifice to measure AVA during analysis after image acquisition, whereas this is not possible on

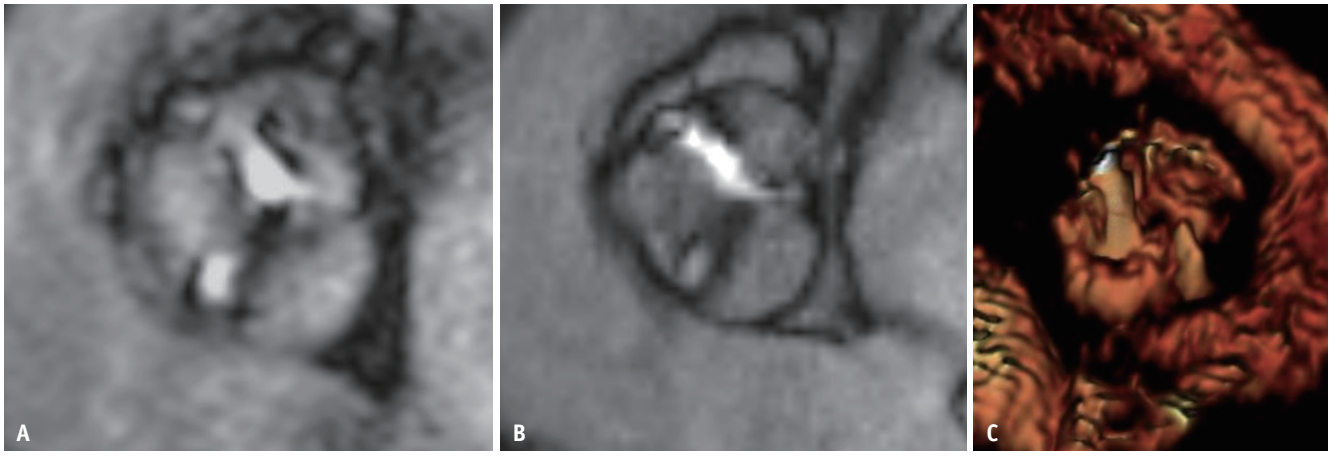

Fig. 8. A representative case with two separate orifices.
The areas for the two orifices were measured twice and summed to calculate the valve area. The 3D planimetry image **(A)** shows better contrast in the valve orifices than in the 2D image **(B)**. Note the bi-cornuate appearance of the flow jet profile on the volume-rendered image **(C)**. 2D = two-dimensional, 3D = three-dimensional

https://doi.org/10.3348/kjr.2020.1218

Korean Journal of Radiology
KJR

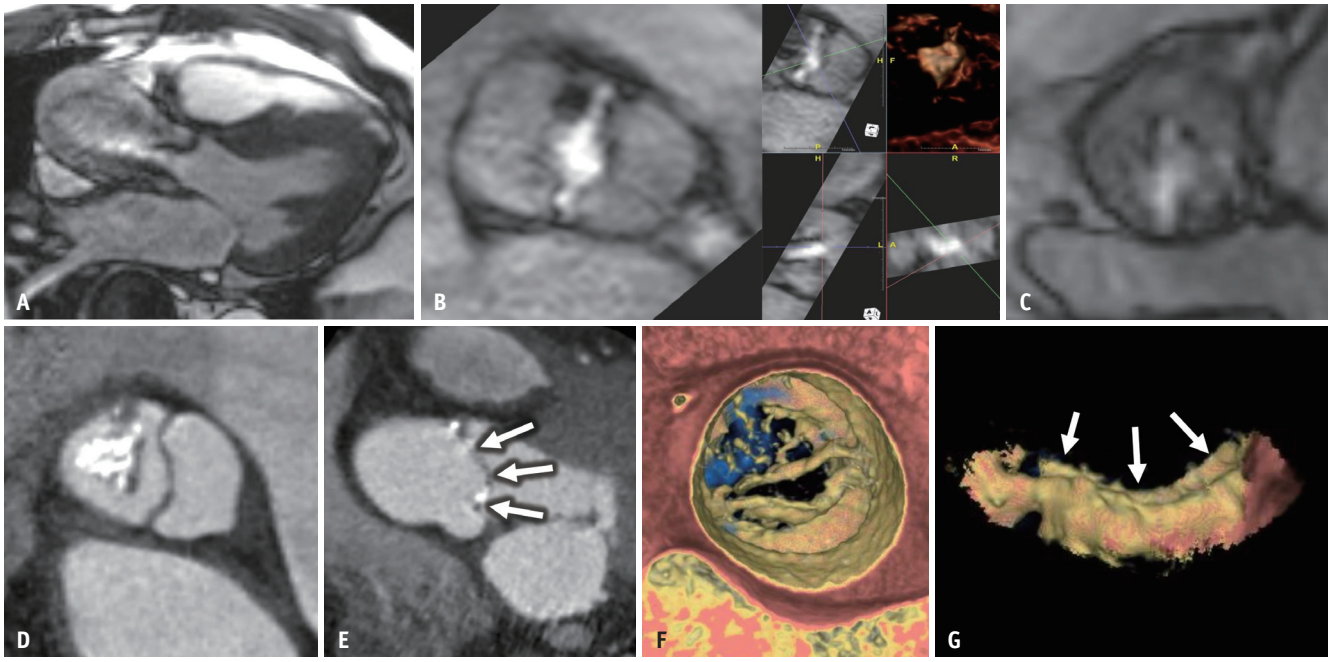

Fig. 9. Comparison of 3D planimetry, 2D planimetry, and CT in a 67-year-old male with calcified bicuspid AV.
There was moderate stenosis on transthoracic echocardiography with an AVA of 1.10 cm^2 (peak velocity, 3.8 m/s; diameter of LVOT, 2.32 cm; velocity-time integral ratio of LVOT [23.3]/AV [88.0], 0.3). The echocardiographic window was rather poor in this study. Cine MRI shows a stenotic jet through the AV in the 3-chamber view **(A)**. The AVA measured with 3D planimetry was 1.18 cm^2 **(B)**. The AVA measured with 2D planimetry was 1.48 cm^2 **(C)**. The peripheral and central parts of the AV orifice could not be measured in a single plane on CT **(D)**. Oblique sagittal reformatted image **(E)** and en-face **(F)** and profile **(G)** navigation images of CT show a curved appearance (arrows) of the AV orifice plane. The AVA was 1.29–1.65 cm^2 on CT. In this patient, 3D planimetry correlated best with echocardiography for measuring AVA. AV = aortic valve, AVA = aortic valve area, LVOT = left ventricular outflow tract, 2D = two-dimensional, 3D = three-dimensional

Table 5. Analysis for the Bicuspid and Tricuspid Aortic Valves

	Bicuspid Aortic Valve	Tricuspid Aortic Valve	*P*
Total patients (n = 139, %)	47 (33.8)	92 (66.2)	
3D			
AVA (cm^2) according to average of OB1 and OB2*	0.79 ± 0.35	0.81 ± 0.46	0.89
Image quality*	3.5 ± 0.4	3.7 ± 0.5	0.72
Agreement with echocardiography	0.92 (95% CI, 0.86–0.96)	0.84 (95% CI, 0.75–0.89)	0.03
2D			
AVA (cm^2) according to average of OB1 and OB2*	0.82 ± 0.37	0.85 ± 0.33	0.87
Image quality*	3.3 ± 0.7	3.4 ± 0.3	0.85
Agreement with echocardiography	0.85 (95% CI, 0.74–0.92)	0.85 (95% 0.77–0.90)	0.90

*Data are mean ± standard deviation. AVA = aortic valve area, CI = confidence interval, OB = observer, 2D = two-dimensional, 3D = three-dimensional

2D cine images that do not permit a change in the cross-section planes of the valve after image acquisition. It can be difficult to prescribe the 2D cine MRI plane exactly along the valve orifice plane because of the continuous movement of the valve and the oblique positioning of the valve orifice plane in some cases. Moreover, 3DP performed within the duration of one breath hold reduces scan time and improves patient workflow, while it theoretically more accurately depicts AVA.

The higher spatial resolution of the 3D technique (2 mm slice thickness), compared with that of the 2D technique (6 mm slice thickness), may allow more reliable AVA measurements. The bright signal intensity due to high-velocity turbulence around and above the jet flow in the aortic valve orifice enables the 3D appearance of the aortic valve jet flow profile to be visualized, facilitating the clear measurement of AVA because of the greater contrast between AVA and the surrounding aortic valve tissue. The

https://doi.org/10.3348/kjr.2020.1218

high contrast in the valve orifices on MR planimetry would be advantageous for measuring AVA compared with CT, which can be limited by low tissue contrast and blooming artifacts when calcifications are present. The stenotic aortic valvular orifices are sometimes difficult to measure on CT or 2D cine MRI, as they may exist in curved planes. Two separate orifices or AVA divisions were only identifiable with MR planimetry, again showing that 3DP may be more accurate than TTE when measuring AVA. Multiple openings were not identified during TTE or surgery, probably because there was no blood flow to fill AV during surgery, and high-degree turbulence and flow acceleration may hinder the identification of multiple orifices with TTE. Furthermore, AVA measurements are not affected by the presence of aortic valve calcifications on cardiovascular MR, but these calcifications may influence the results obtained using CT or echocardiography.

Peak systolic velocity measurements on VENC MRI and 3DP or 2DP indicated a moderate but statistically significant negative linear correlation, but the correlation showed a slightly more negative tendency for 3DP than on 2DP.

Echocardiographic AVA determination using the continuity equation is dependent on the LVOT measurement. However, the exact LVOT area is not directly measured on TTE, and it should be inferred, instead, from the LVOT diameter, which can produce errors because of the ovoid appearance of the LVOT. Therefore, in cases of a limited acoustic window and abundant calcification, 3DP can be used as an alternative for estimating AVA. The use of 3DP is particularly beneficial when evaluating AS in patients with two separate orifices, several divided sections, or complex flow velocity profiles. In cases with two or more separate orifices, the estimation of AVA using echocardiography can be erroneous, unless all orifices are evaluated for AVA measurement. 3D appearances of high-velocity jets on 3D MRI help in understanding the hemodynamic characteristics of aortic valve stenosis, including the presence of separate stenotic ostia not revealed by echocardiography. It may also play a role in the pre-procedural or follow-up evaluation of patients undergoing transcatheter aortic valve implantation [21].

To date, direct 2DP of the aortic valve orifice has been the most useful technique for quantifying stenosis severity [7,22], and it is typically performed by placing an imaging plane through the valve tips during systole [23]. However, it is important to ensure that the image slice is thin and precisely located at the valve tips, and multiple parallel thin slices are acquired parallel to the valve orifice. If a large amount of calcification is present in the aortic valve, it can be difficult to identify the true orifice. In 2DP, measurement errors can result from severely calcified aortic valves. In contrast, 3DP is less affected by AV calcification.

Our study has limitations. First, there was no gold standard comparison group; however, it is equally important to note that no definitive method exists for the *in vivo* evaluation of AVA. We did not opt to perform an invasive evaluation of AVA-by applying the Gorlin formula to catheterization data as an alternative to TTE, but we identified a strong correlation between the 3DP and echocardiographic parameters. More importantly, 3DP could accurately detect severe AS identified by echocardiography. Second, in our study, the image acquisition duration was 190 ms, but to achieve a better temporal resolution, we needed a shorter acquisition time. Third, 3D echocardiography provides an accurate assessment of the AVA by providing the anatomy of the LVOT. However, we have used 2D echocardiography instead of 3D echocardiography.

In conclusion, our 3DP method was fast, reproducible, and useful for interpreting the MRI data of both controls and patients with moderate-to-severe AS. High-resolution 3D MR image acquisition, with single-breath-hold SSFP sequences, gave AVA measurement with low observer variability that correlated highly with those obtained by echocardiography. We propose that 3DP can be used to assess the severity of AS in clinical practice.

Supplement

The Supplement is available with this article at https://doi.org/10.3348/kjr.2020.1218.

Supplementary Movie Legends

Movie The movie shows the procedure for measuring the aortic valve area using 3D MRI data and software (Aquaris iNtuition, TeraRecon).

Conflicts of Interest

The authors have no potential conflicts of interest to disclose.

Acknowledgments

We appreciate Mr. Wooin Jung, RT, for his excellent

technical supports.

Author Contributions

Conceptualization: Hae Jin Kim, Yeon Hyeon Choe. Data curation: Hae Jin Kim, Yeon Hyeon Choe. Formal analysis: Hae Jin Kim, Yeon Hyeon Choe. Funding acquisition: Yeon Hyeon Choe. Investigation: Hae Jin Kim, Yeon Hyeon Choe, Eun Kyoung Kim, Mirae Lee, Sung-Ji Park. Methodology: Hae Jin Kim, Yeon Hyeon Choe, Sung Mok Kim. Project administration: Hae Jin Kim, Yeon Hyeon Choe. Resources: Yeon Hyeon Choe, Joonghyun Ahn, Keumhee C. Carriere. Software: Hae Jin Kim, Yeon Hyeon Choe. Supervision: Yeon Hyeon Choe. Validation: Hae Jin Kim, Yeon Hyeon Choe, Joonghyun Ahn, Keumhee C. Carriere. Visualization: Hae Jin Kim, Yeon Hyeon Choe. Writing—original draft: Hae Jin Kim, Yeon Hyeon Choe. Writing—review & editing: Yeon Hyeon Choe.

ORCID iDs

Hae Jin Kim
https://orcid.org/0000-0002-5692-3248
Yeon Hyeon Choe
https://orcid.org/0000-0002-9983-048X
Sung Mok Kim
https://orcid.org/0000-0001-5190-2328
EunKyoung Kim
https://orcid.org/0000-0002-7653-3503
Mirae Lee
https://orcid.org/0000-0003-4142-5403
Sung-Ji Park
https://orcid.org/0000-0002-7075-847X
Joonghyun Ahn
https://orcid.org/0000-0002-5768-5990
Keumhee C. Carriere
https://orcid.org/0000-0001-6273-4825

REFERENCES

1. van der Linde D, Rossi A, Yap SC, McGhie JS, van den Bosch AE, Kirschbaum SW, et al. Ascending aortic diameters in congenital aortic stenosis: cardiac magnetic resonance versus transthoracic echocardiography. *Echocardiography* 2013;30:497-504
2. Nickl W, Füth R, Smettan J, Köhler T, Lankisch M, Kramer F, et al. Assessment of aortic valve area combining echocardiography and magnetic resonance imaging. *Arq Bras Cardiol* 2012;98:234-242
3. Pontone G, Andreini D, Bartorelli AL, Bertella E, Mushtaq S, Gripari P, et al. Comparison of accuracy of aortic root annulus assessment with cardiac magnetic resonance versus echocardiography and multidetector computed tomography in patients referred for transcatheter aortic valve implantation. *Am J Cardiol* 2013;112:1790-1799
4. Altiok E, Frick M, Meyer CG, Al Ateah G, Napp A, Kirschfink A, et al. Comparison of two- and three-dimensional transthoracic echocardiography to cardiac magnetic resonance imaging for assessment of paravalvular regurgitation after transcatheter aortic valve implantation. *Am J Cardiol* 2014;113:1859-1866
5. Garcia J, Capoulade R, Le Ven F, Gaillard E, Kadem L, Pibarot P, et al. Discrepancies between cardiovascular magnetic resonance and Doppler echocardiography in the measurement of transvalvular gradient in aortic stenosis: the effect of flow vorticity. *J Cardiovasc Magn Reson* 2013;15:84
6. Hamm K, Trinkmann F, Heggemann F, Gruettner J, Schmid-Bindert G, Borggrefe M, et al. Evaluation of aortic valve stenosis using a hybrid approach of Doppler echocardiography and inert gas rebreathing. *In Vivo* 2012;26:1027-1033
7. Speiser U, Quick S, Haas D, Youssef A, Waessnig NK, Ibrahim K, et al. 3-T magnetic resonance for determination of aortic valve area: a comparison to echocardiography. *Scand Cardiovasc J* 2014;48:176-183
8. Singh A, McCann GP. Cardiac magnetic resonance imaging for the assessment of aortic stenosis. *Heart* 2019;105:489-497
9. Choe YH, Kim SM, Park SJ. Computed tomography and magnetic resonance imaging assessment of aortic valve stenosis: an update. *Precis Future Med* 2020;4:119-132
10. Kim MY, Park EA, Lee W, Lee SP. Cardiac magnetic resonance feature tracking in aortic stenosis: exploration of strain parameters and prognostic value in asymptomatic patients with preserved ejection fraction. *Korean J Radiol* 2020;21:268-279
11. Bak SH, Kim SM, Park SJ, Kim MY, Kim HJ, Lee SC, et al. Semiautomated analysis of aortic stenosis parameters on velocity-encoded phase-contrast MR images in patients with severe aortic stenosis: a comparison with echocardiography. *Cardiovasc Imaging Asia* 2017;1:78-85
12. Lee JW, Hur JH, Yang DH, Lee BY, Im DJ, Hong SJ, et al. Guidelines for cardiovascular magnetic resonance imaging from the Korean Society of Cardiovascular Imaging—Part 2: interpretation of cine, flow, and angiography data. *Cardiovasc Imaging Asia* 2019;3:113-124
13. Jo Y, Kim J, Park CH, Lee JW, Hur JH, Yang DH, et al. Guidelines for cardiovascular magnetic resonance imaging from Korean Society of Cardiovascular Imaging (KOSCI) - Part 1: standardized protocol. *Investig Magn Reson Imaging* 2019;23:296-315
14. Tanaka K, Makaryus AN, Wolff SD. Correlation of aortic valve area obtained by the velocity-encoded phase contrast continuity method to direct planimetry using cardiovascular magnetic resonance. *J Cardiovasc Magn Reson* 2007;9:799-805
15. Pouleur AC, le Polain de Waroux JB, Pasquet A, Vancraeynest D, Vanoverschelde JL, Gerber BL. Planimetric and continuity

equation assessment of aortic valve area: head to head comparison between cardiac magnetic resonance and echocardiography. *J Magn Reson Imaging* 2007;26:1436-1443
16. Dimitriou P, Kähäri A, Emilsson K, Thunberg P. Cardiovascular magnetic resonance imaging and transthoracic echocardiography in the assessment of stenotic aortic valve area: a comparative study. *Acta Radiol* 2012;53:995-1003
17. Song I, Park JA, Choi BH, Ko SM, Shin JK, Chee HK, et al. Morphological and functional evaluation of quadricuspid aortic valves using cardiac computed tomography. *Korean J Radiol* 2016;17:463-471
18. John AS, Dill T, Brandt RR, Rau M, Ricken W, Bachmann G, et al. Magnetic resonance to assess the aortic valve area in aortic stenosis: how does it compare to current diagnostic standards? *J Am Coll Cardiol* 2003;42:519-526
19. Ahn JH, Kim SM, Park SJ, Jeong DS, Woo MA, Jung SH, et al. Coronary microvascular dysfunction as a mechanism of angina in severe AS: prospective adenosine-stress CMR study. *J Am Coll Cardiol* 2016;67:1412-1422
20. Tandon A, Grayburn PA. Imaging of low-gradient severe aortic stenosis. *JACC Cardiovasc Imaging* 2013;6:184-195
21. Fairbairn TA, Steadman CD, Mather AN, Motwani M, Blackman DJ, Plein S, et al. Assessment of valve haemodynamics, reverse ventricular remodelling and myocardial fibrosis following transcatheter aortic valve implantation compared to surgical aortic valve replacement: a cardiovascular magnetic resonance study. *Heart* 2013;99:1185-1191
22. Buchner S, Debl K, Schmid FX, Luchner A, Djavidani B. Cardiovascular magnetic resonance assessment of the aortic valve stenosis: an in vivo and ex vivo study. *BMC Med Imaging* 2015;15:34
23. Myerson SG. Heart valve disease: investigation by cardiovascular magnetic resonance. *J Cardiovasc Magn Reson* 2012;14:7

https://doi.org/10.3348/kjr.2020.1218